Direct *para*-selective C-H Amination of Benzyl Alcohols: Selectivity Independent of Side Substituents

Donghan Liu[1], Ting Tu[1], Tinglei Zhang[1], Guihua Nie[1], Tianhui Liao[1], Shi-Chao Ren[1,*], Xinglong Zhang[2,*], Yonggui Robin Chi[1,3,*]

[1] State Key Laboratory of Green Pesticide, Key Laboratory of Green Pesticide and Agricultural Bioengineering, Ministry of Education, Center for R&D of Fine Chemicals of Guizhou University, Guiyang, 550025, China.

[2] Institute of High Performance Computing, A*STAR (Agency for Science, Technology and Research) Singapore 138632 (Singapore).

[3] School of Chemistry, Chemical Engineering, and Biotechnology, Nanyang Technological University, Singapore, 637371, Singapore.

*Corresponding author. Email: scren@gzu.edu.cn; Zhang_Xinglong@ihpc.a-star.edu.sg; robinchi@ntu.edu.sg

Supporting Information

Table of contents

II. Computational details

II.1 Computational Methods

Density functional theory (DFT) calculations were performed using *Gaussian 16* rev. B.01 software,[1] in the gas phase using the hybrid meta exchange-correlation M06-2X[2] functional and the def2-SVP[3,4] basis set for all atoms. The M06-2X functional[1] was chosen as it gives the best agreement with the experimental redox potential values amongst 8 functionals tested for the study of computational redox potential calculations.[2] In addition, in a study of both experimental and computational electrochemical potentials for over 180 organic substrates, M06-2X functional gives an R^2 value of 0.97 for the correlation between the experimental and calculated redox potentials,[3] implying that M06-2X functional performs well for studying organic radical species. For radical systems and the openshell singlet system, the DFT calculations were performed within the unrestricted formalism using the unrestricted Kohn-Sham (UKS) theory. Furthermore, for the openshell singlet diradical system involved in the radical-radical coupling step, the keyword "guess=mix" was used to ensure that unrestricted Hartree-Fock (UHF) wavefunction for singlet state is used. The keyword "stable=opt" was used to ensure that the resulting wavefunction is stable with respect to an unrestricted wavefunction, as we expect the radical-radical coupling transition structure to possess significant diradical character.
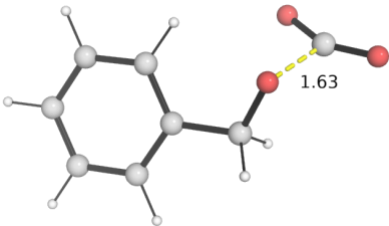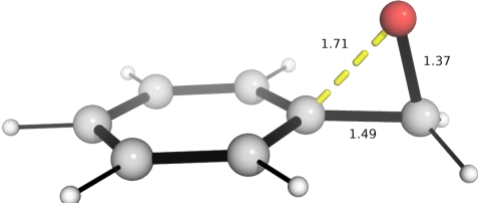
Minima and transition structures on the potential energy surface (PES) were confirmed as such by harmonic frequency analysis, showing respectively zero and one imaginary frequency. Gibbs energies were evaluated at the reaction temperature of 20 °C and corrected for zero-point vibrational energies at the same level of theory, using Grimme's scheme of quasi-RRHO treatment of vibrational entropies[5], using the GoodVibes code[6]. Vibrational entropies of frequencies below 100 cm^{-1} were obtained according to a free rotor description, using a smooth damping function to interpolate between the two limiting descriptions.[5] The free energies reported in *Gaussian* from gas-phase optimization were further corrected using standard concentration of 1 mol/L,[7] which were used in solvation calculations, instead of the gas-phase 1atm used by default in

the *Gaussian* program.

To improve on the accuracy of the corrected Gibbs energy profile, single point (SP) calculations on the gas phase M06-2X/def2-SVP optimized geometries were performed at M06-2X with def2-TZVP[3,8] basis set for all atoms in the implicit SMD continuum solvation model[9] for acetonitrile solvent that was used experimentally, to account for the effect of solvent on the potential energy surface. The final corrected Gibbs energy SMD(acetonitrile)-M06-2X/def2-TZVP//M06-2X/def2-SVP is used for discussion throughout. All Gibbs energy values in the text and figures are quoted in kcal mol^{-1}.

Non-covalent interactions (NCIs) were analyzed using NCIPLOT[10] calculations. The *.wfn* files for NCIPLOT were generated at M06-2X/def2-SVP level of theory. NCI indices calculated with NCIPLOT were visualized at a gradient isosurface value of *s = 0.5* au. These are colored according to the sign of the second eigenvalue (λ_2) of the Laplacian of the density ($\nabla^2\rho$) over the range of –0.1 (blue = attractive) to +0.1 (red = repulsive). All molecular structures and plots were visualized using *PyMOL* software.[11] Spin density plots are visualized using an isosurface value of 0.005 au throughout.

II.2 Optimized DFT structures

TS1	TS2
$\Delta G^{\ddagger} = 11.4$	$\Delta G^{\ddagger} = -4.0$
TS3	TS3-c2
$\Delta G^{\ddagger} = 6.0$	$\Delta G^{\ddagger} = 7.4$

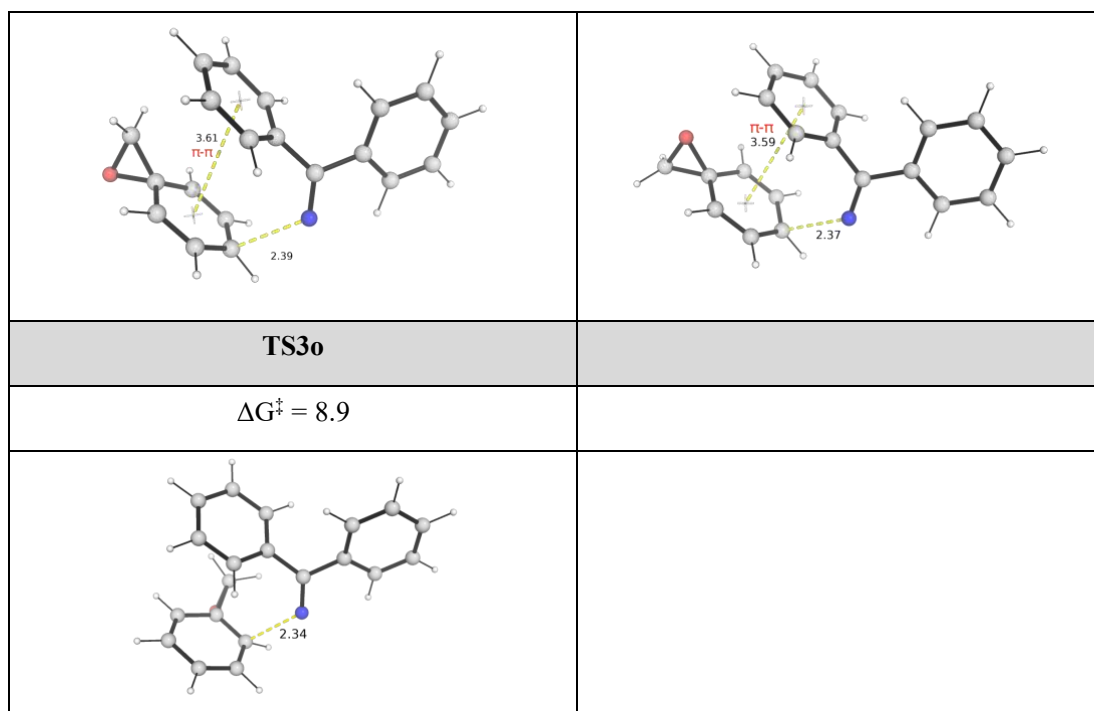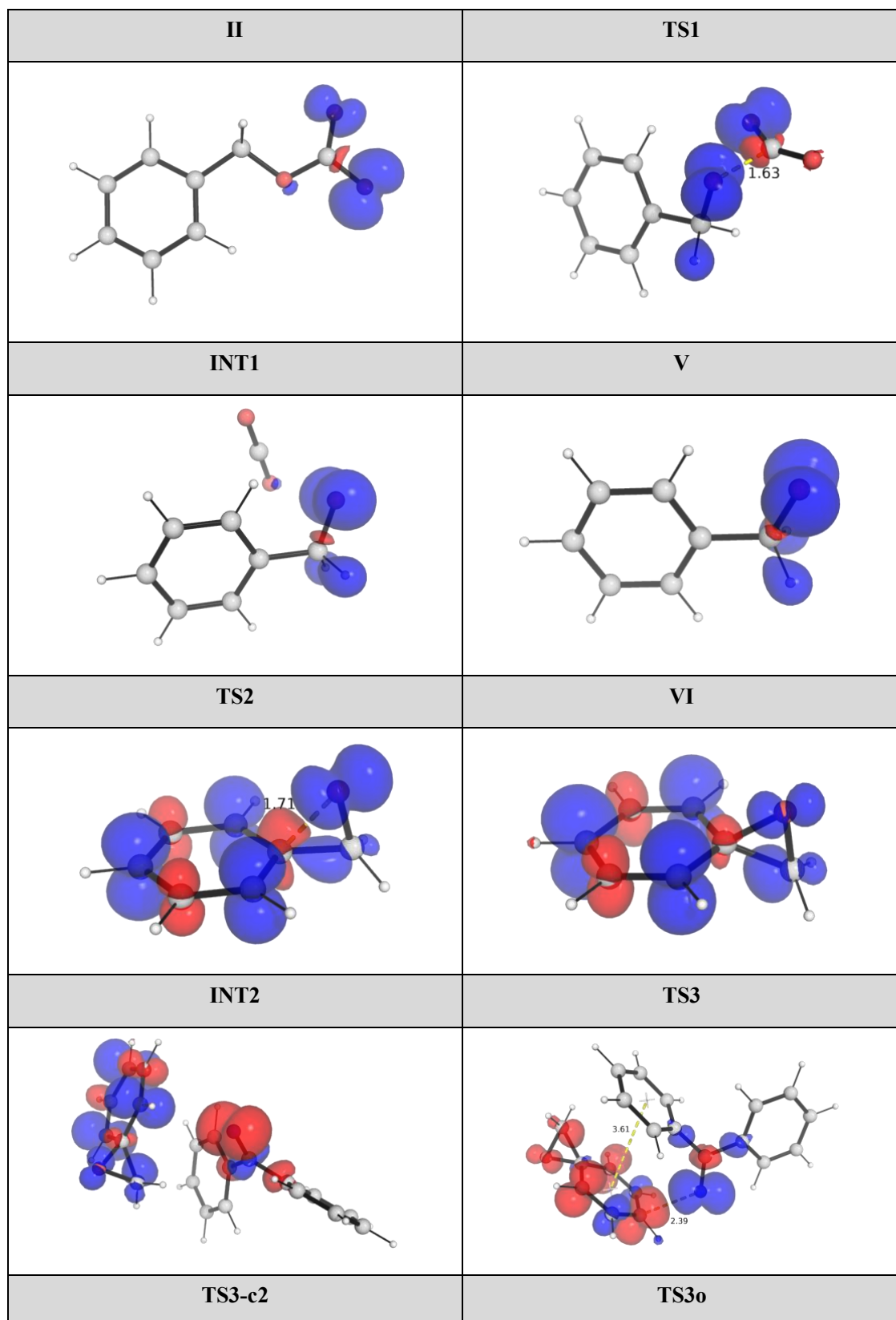|	
TS3o	
$\Delta G^{\ddagger} = 8.9$	

Figure S1. DFT optimized structures for key transition states (TSs). Bond distances are given in Å. Gibbs energy are relative to species **II** as reference.

DFT-optimized structures for the transition states (TSs) are shown in Figure S1. For the radical cross-coupling step forming the C–N bond, two TS conformers, **TS3** and **TS3-c2**, were found. These two differ in the orientation of the epoxide oxygen: the TS with epoxide oxygen facing the phenyl ring of the imine radical (**TS3-c2**) has a higher barrier, by 1.4 kcal/mol, than the one with oxygen atom facing away from the phenyl ring of the imine radical (**TS3**). The higher barrier possibly results from the electron repulsion between the oxygen lone pairs and the π-system of the aromatic ring.

For the C–N coupling at the ortho-position (**TS3o**), this TS has a barrier that is 2.9 kcal/mol higher than **TS3**, as it does not benefit from π-π interaction between the aromatic rings.

II.3 Spin density plots

The spin density plots for various species are shown in Figure S2. For the decarboxylation of species II, we can visualize the radical movement by looking at TS1. Upon decarboxylation, the radical is localized on the phenyl methanolate whereas the CO_2 molecule becomes neutral and has no radical characteristic (**INT1**).

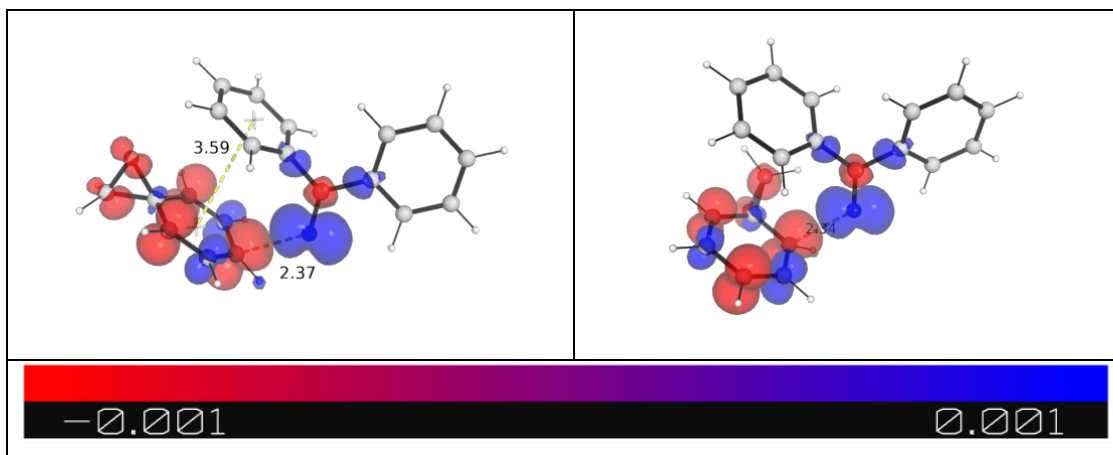| II	TS1
	1.63
INT1	**V**
TS2	**VI**
1.71	
INT2	**TS3**
	3.61 / 2.39
TS3-c2	**TS3o**

Figure S2. Spin density plots for openshell species at an isosurface value of 0.005 au

Species **X** has almost similar radical characteristics at the ortho and para carbon atoms and the radical positions for the radical cross coupling at the para-position (**TS3**) is almost similar to the radical cross coupling at the ortho-position (**TS3o**). The regioselective favorability for para over ortho results from the presence of non-covalent π-π interaction present in **TS3** but absent in **TS3o**.
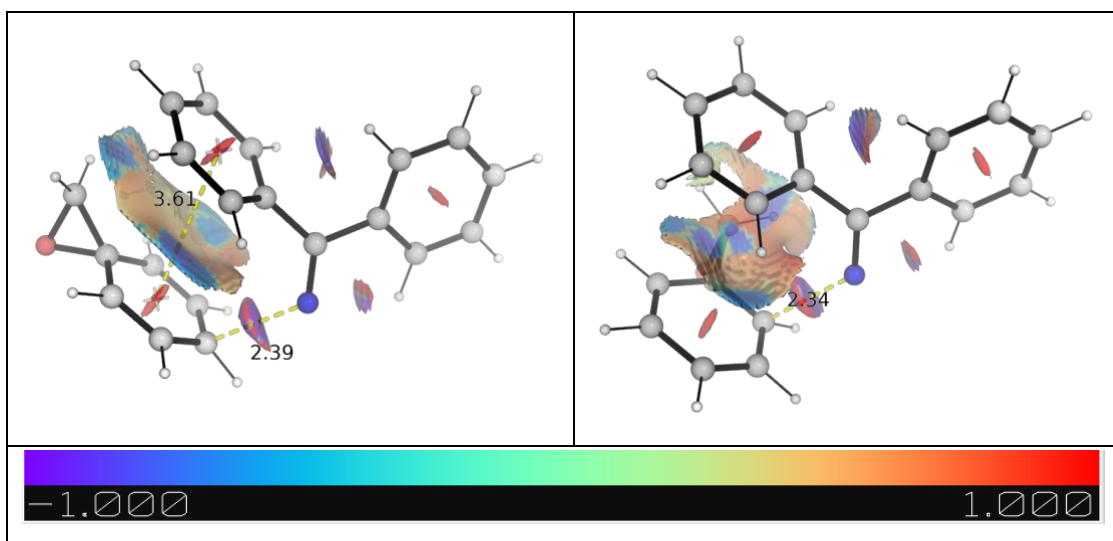

Figure S3. Non-covalent interaction (NCI) plots (bottom) for **TS3** and **TS3o**. Structures used are DFT-optimized structures, with key bond distances given in Å. NCI plots were visualized at a gradient isosurface value of *s = 0.5* au.

II.4 Determination of selectivity ratio using simple transition state theory

The Eyring equation

$$k = \frac{k_{\mathrm{B}}T}{h}\mathrm{e}^{-\Delta G^{\ddagger}/RT}$$

gives the rate constant under simple transition state theory (TST) assumptions.

Under kinetic control, as we compare the barrier heights difference between competing transition states, the product selectivity is given by:

$$\frac{k_A}{k_B} = \frac{e^{-\Delta G_A^{\ddagger}/RT}}{e^{-\Delta G_B^{\ddagger}/RT}} = e^{-\Delta\Delta G^{\ddagger}/RT}$$

where k_X is the rate constant of pathway X (X=A or B); $\Delta G_X^{\ddagger}$ is the activation barrier for pathway X; and $\Delta\Delta G_X^{\ddagger}$ is the difference in the barrier heights; and R is the gas constant, T the temperature. Note that the Eyring Equation pre-exponential factor cancels when comparing the ratio of the rate constants. Thus, using the calculated $\Delta\Delta G_X^{\ddagger}$ value of 2.9 kcal/mol (difference of barrier heights between the regioslective TSs: the TS for *para*-position radical cross coupling and *ortho*-position radical cross coupling) at 20ºC (293.15K), we obtained the selectivity ratio of about 145 : 1.

II.5 Regioselectivity outcome for substrates giving products 2i, 2l, 2r and 2t

To consider the effect of electron-withdrawing and electron donating groups on the regioselective outcome, we performed DFT calculations on the regioselectivity step for the substrate giving product **2i, 2l, 2r** and **2t**.

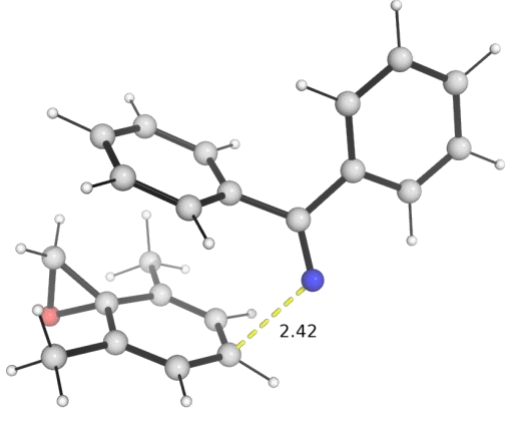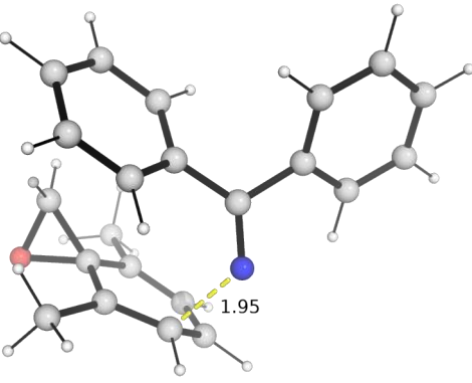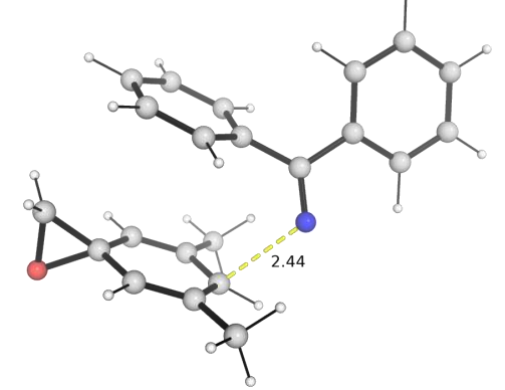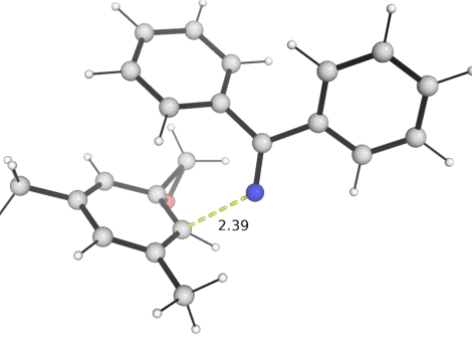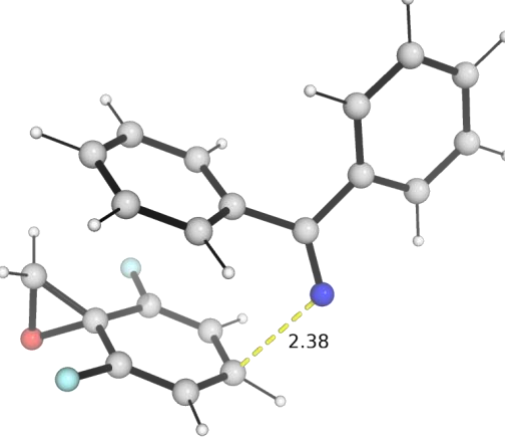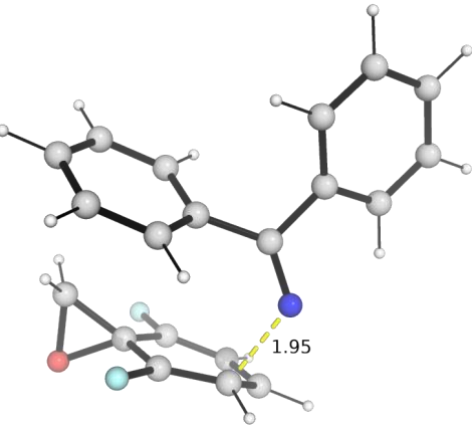DFT computations show that for the electron-donating methyl substituent at the *ortho*-position forming product **2i**, the TS forming the *para* product (**TS2i_para**) is favored over the TS forming the *meta* product (**TS2i_meta**) by 23.7 kcal/mol, whereas for the electron-donating methyl substituent at the *meta*-position forming product **2r**, the TS forming the *para* product (**TS2r_para**) is favored over that forming the *ortho* product (**TS2r_ortho**) by 3.6 kcal/mol.

Similarly, for the electron-withdrawing F substituent at the *ortho*-position forming product **2l**, the TS forming the *para* product (**TS2l_para**) is favored over the TS forming the *meta* product (**TS2l_meta**) by 24.2 kcal/mol, whereas for the electron-withdrawing F substituent at the *meta*-position forming product **2t**, the TS forming the *para* product (**TS2t_para**) is favored over that forming the *ortho* product (**TS2t_ortho**) by 1.1 kcal/mol.

We note that the formation of C–N bond via radical-radical coupling at the *meta*-position is highly unfavorable due to that the spins at the *meta*-position and the nitrogen atom are both parallel, whereas the spins are opposite between the radical at the nitrogen atom and the *para*- or *ortho*-position.

DFT optimized structures and the barrier height differences are given in Figure S4.

TS2i_para	TS2i_meta
$\Delta\Delta G^{\ddagger} = 0.0$	$\Delta\Delta G^{\ddagger} = 23.7$

TS2r_para	TS2r_ortho
$\Delta\Delta G^{\ddagger} = 0.0$	$\Delta\Delta G^{\ddagger} = 3.6$

TS2l_para	TS2l_meta
$\Delta\Delta G^{\ddagger} = 0.0$	$\Delta\Delta G^{\ddagger} = 24.2$

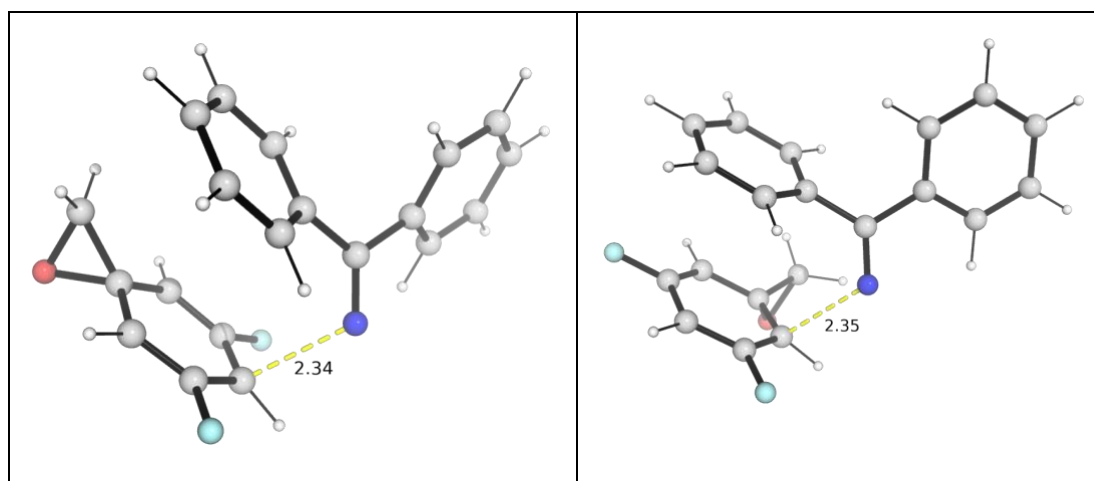| TS2t_para	TS2t_ortho
$\Delta\Delta G^{\ddagger} = 0.0$	$\Delta\Delta G^{\ddagger} = 1.1$

Figure S4. DFT optimized structures for the transition states (TSs) for the regioselectivity determining step for selected substrates. Bond distances are given in Å. Gibbs energy are relative to the lowest barrier TS structure within each substrate.**II.6 Optimized structures and absolute energies**

Geometries of all optimized structures (in *.xyz* format with their associated gas-phase energy in Hartrees) are included in a separate folder named *DFT_structures*. All these data have been deposited and uploaded to https://zenodo.org/records/12770031 (DOI: 10.5281/zenodo.12770031).

Absolute values (in Hartrees) for SCF energy, zero-point vibrational energy (ZPE), enthalpy and quasi-harmonic Gibbs free energy (at 20ºC/393.15 K) for optimized structures are given below. Single point corrections in SMD acetonitrile using M06-2X/def2-TZVP level of theory are also included.

Table S1 Optimized structures and absolute energies, zero-point energies

Structure	E/au	ZPE/au	H/au	T.S/au	qh-G/au	SP SMD(MeCN)-M06-2X/def2-TZVP
co2	-188.37047	0.012131	-188.35485	0.020809	-188.37566	-188.59714
imine_ra dical	-555.44934	0.192575	-555.24537	0.046072	-555.29007	-556.07624
II	-	0.136511	-533.91222	0.044963	-	-534.68141

	534.05894				533.95503	
TS1	-534.03449	0.134055	-533.89038	0.043943	-533.93246	-534.66133
INT1	-534.07277	0.132721	-533.92849	0.047651	-533.97376	-534.69696
V	-345.6936	0.119414	-345.56657	0.036414	-345.60231	-346.09471
TS2	-345.66838	0.119697	-345.5418	0.034124	-345.57592	-346.07395
VI	-345.67554	0.120271	-345.54823	0.034368	-345.58253	-346.07736
INT2	-901.13714	0.313644	-900.80409	0.065837	-900.86529	-902.16127
TS3	-901.13314	0.314304	-900.8004	0.062658	-900.85937	-902.15641
TS3-c2	-901.13434	0.314376	-900.80158	0.062061	-900.86029	-902.15434
VII	-901.21054	0.319388	-900.87332	0.060409	-900.93074	-902.22953
2a	-901.28486	0.319786	-900.94637	0.063839	-901.00603	-902.30614
TS3o	-901.12977	0.314117	-900.79729	0.061815	-900.85591	-902.15179
TS_2i_para	-979.67499	0.370279	-979.28347	0.067979	-979.34753	-980.78379
TS_2i_meta	-979.63703	0.369461	-979.24638	0.06721	-979.31025	-980.74527
TS_2l_para	-1099.4004	0.298938	-1099.0815	0.066113	-1099.1435	-1100.6616
TS_2l_meta	-1099.3627	0.298102	-1099.0447	0.065359	-1099.1065	-1100.6224
TS_2r_para	-979.67209	0.369446	-979.28102	0.068574	-979.34599	-980.78264

TS_2r_or tho	-979.6674	0.369082	-979.27661	0.069006	-979.34182	-980.77633
TS_2t_pa ra	-1099.3979	0.298163	-1099.0798	0.065895	-1099.1418	-1100.6617
TS_2t_ort ho	-1099.3964	0.297792	-1099.0785	0.065818	-1099.1406	-1100.6596

IX. References and note

[1] Frisch, M. J. .; Trucks, G. W. .; Schlegel, H. B. .; Scuseria, G. E. .; Robb, M. A. .; Cheeseman, J. R. .; Scalmani, G. .; Barone, V. .; Petersson, G. A. .; Nakatsuji, H. .; et al. Gaussian 16, Revision B.01. 2016.

[2] Zhao, Y.; Truhlar, D. G. The M06 Suite of Density Functionals for Main Group Thermochemistry, Thermochemical Kinetics, Noncovalent Interactions, Excited States, and Transition Elements: Two New Functionals and Systematic Testing of Four M06-Class Functionals and 12 Other Function. *Theor. Chem. Acc.* **2008**, *120* (1), 215–241.

[3] Weigend, F.; Ahlrichs, R. Balanced Basis Sets of Split Valence, Triple Zeta Valence and Quadruple Zeta Valence Quality for H to Rn: Design and Assessment of Accuracy. *Phys. Chem. Chem. Phys.* **2005**, *7* (18), 3297–3305.

[4] Weigend, F. Accurate Coulomb-Fitting Basis Sets for H to Rn. *Phys. Chem. Chem. Phys.* **2006**, *8* (9), 1057–1065.

[5] Grimme, S. Supramolecular Binding Thermodynamics by Dispersion-Corrected Density Functional Theory. *Chem.: Eur. J.* **2012**, *18* (32), 9955–9964.

[6] Luchini, G.; Alegre-Requena, J. V.; Funes-Ardoiz, I.; Paton, R. S.; Pollice, R. GoodVibes: Automated Thermochemistry for Heterogeneous Computational Chemistry Data. **2020**, *9*, 291.

[7] Bryantsev, V. S.; Diallo, M. S.; Goddard Iii, W. A.; Goddard, W. A. Calculation of Solvation Free Energies of Charged Solutes Using Mixed Cluster/Continuum Models. *J. Phys. Chem. B* **2008**, *112* (32), 9709–9719.

[8] Hellweg, A.; Rappoport, D. Development of New Auxiliary Basis Functions of the Karlsruhe Segmented Contracted Basis Sets Including Diffuse Basis Functions (Def2-SVPD, Def2-TZVPPD, and Def2-QVPPD) for RI-MP2 and RI-CC Calculations. *Phys. Chem. Chem. Phys.* **2014**, *17* (2), 1010–1017.

[9] Marenich, A. V.; Cramer, C. J.; Truhlar, D. G. Universal Solvation Model Based on Solute Electron Density and on a Continuum Model of the Solvent Defined by the Bulk Dielectric Constant and Atomic Surface Tensions. *J. Phys. Chem. B* **2009**, *113* (18), 6378–6396.

[10] Contreras-García, J.; Johnson, E. R.; Keinan, S.; Chaudret, R.; Piquemal, J. P.; Beratan, D. N.; Yang, W. NCIPLOT: A Program for Plotting Noncovalent Interaction Regions. *J. Chem. Theory Comput.* **2011**, *7* (3), 625–632.

[11] Schrödinger, L. *The PyMOL Molecular Graphics Development Component, Version 1.8*; **2015.**

[12] G. Bertolini, G. Pavich and B. Vergani, A New Simple One-Pot Regioselective

Preparation of Mixed Diesters of Carbonic Acid. *J. Org. Chem.* **1998**, *63* (17), 6031–6034.

[13] R. T. McBurney, A. D. Harper, A. M. Z. Slawin, J. C. Walton, An all-purpose preparation of oximecarbonates and resultant insights into the chemistry of alkoxycarbonyloxyl radicals. *Chem. Sci.*, **2012**, *3*, 3436-3444.

[14] H-D. Qian, Z-H Li, S. Deng, C. Yao, H-M Xiang, G. Xu, Z-Q Geng, Z. Wang, L. Chen, C. Liu, C. Zhu, X. Qi, H. Xu, Catalytic Asymmetric Vinylogous and Bisvinylogous Propargylic Substitution. *J. Am. Chem. Soc.* **2022**, *144* (34), 15779–15785.

[15] S. Mandal, T. Paul, P. Karjee, M. Barman, T. Punniyamurthy. Site-Selective C8-Alkylation of Quinolines with Cyclopropanols: Merging C-H/C-C BondActivation. *Org. Lett.* **2023,** *25 (*43), 7805–7809.

[16] CCDC 2314816 contain the supplementary crystallographic data for compound **2a**. These data can be obtained free of charge from The Cambridge Crystallographic Data Center *via* www.ccdc.cam.ac.uk/data_request/cif.

[17] S. Ghosh, U. Maitra. Adaptive Dendron: A Bile Acid Oligomer Behaving as Both Normal and Inverse Micellar Mimic. *Org. Lett.* **2006**, *8* (3), 399-402.